HIGH-POWER 20-CHANNEL NEODYMIUM GLASS LASER AND COMBINED LASER AND BEAM HEATING OF A PLASMA

Ya. V. Afanas'ev, N. G. Basov, V. A. Gribkov,
A. I. Isakov, N. V. Kalachev, O. N. Krokhin,
L. V. Krupnova, V. Ya. Nikulin, V. V. Pustovalov,
A. B. Romanov, M. A. Savchenko, O. G. Semenov,
V. P. Silin, and G. V. Sklizkov

A high-power 20-channel neodymium-glass laser is described (energy $\sim$ 1 kJ, pulse duration 2 nsec). It is part of the "Flora" facility intended for combined simultaneous heating of a plasma by powerful laser radiation (PLR) and by a relativistic electron beam (REB) produced in a facility of the "plasma focus" type. The paper deals theoretically with the processes of combined interaction of PLR and REB with a current plasma and a solid target.

INTRODUCTION

Following the suggestion of using powerful laser radiation (PLR) to heat matter to thermonuclear temperatures [1], many theoretical papers have formulated the conditions for the feasibility of a thermonuclear reaction with positive energy yield in a plasma obtained by focusing the PLR on targets of special construction [2, 3]. Somewhat later, research was initiated on the possibility of obtaining controlled thermonuclear fusion (CTF) by heating a solid target with a powerful relativistic electron beam (REB) [4, 5]. The main expectation was the realization of classical absorption of the REB in the heavy shells of the targets [6, 7].

By now, many experimental results have been obtained on the efficiency of heating a superdense plasma with the aid of PLR [8-10]. However, the efficiencies of the existing lasers suitable for use in laser driven thermonuclear fusion (LTF) do not exceed several percent. On the other hand, although the efficiencies with REB can in principle be quite high, many difficulties are encountered in this method of obtaining a thermonuclear plasma, particularly with focusing the beam and guiding it to the target, as well as with the absorption of the REB in the target. Effective heating by the backward flow of the solid-target material, which might contribute to excitation, in the target, of collective processes of interaction of the REB with the plasma, calls for the construction of installations in which the current density exceeds by four or five orders of magnitude the density attainable at the present time [7].

To make simultaneous use of the advantages of both heating methods, a scheme was proposed of combined laser and beam heating (CLBH) of a solid target, wherein the laser prepares the initial plasma, which is subsequently heated by an REB pulse that carries the bulk of the energy [11]. It was proposed to use a "plasma focus" (PF) [12, 13] as the source of the REB.

The present investigation was carried out with an aim at developing a powerful pulsed source of neutrons, x rays, and plasma-particle streams, suitable for work on the engineering problems of pulsed thermonuclear reactors and on neutron physics.

We report in the article the theoretical premises of the development of such a source based on combined laser and beam heating of a plasma, and describe the laser part of the "Flora" facility (laser and "plasma focus"), intended for the realization of CLBH.

It is of interest to also use the plasma focus (PF) at the instant of compression [13] as a source for the PLR. In this case, by varying the shape and duration of the PLR pulse, it is possible to investigate independently various parametric mechanisms of the interaction

of electromagnetic radiation with plasma [14] under conditions that are convenient for comparison with the theory.

Taking the foregoing into account, the laser intended for the interaction with the PF and for the CLBH must possess the following parameters:

1. The energy in the pulse must be of the order of or higher than the thermal energy of the PF in the first compression ($\sim$ 100 J), but can be less than the REB energy ($\sim$ 10 kJ) [12].

2. The laser pulses must be variable within a range from $(2-3) \cdot 10^{-8}$ sec (in which case it is rectangular in shape and is intended to heat the PF plasma via the inverse bremsstrahlung mechanism) down to short spikes of duration 10^{-11}–10^{-9} sec (for the investigation of the parametric mechanism of the interaction between the PLR and the plasma).

3. The required contrast of the radiation is relatively low, 10^3, since there is no danger of target evaporation as in the case of a laser plasma [8, 15, 16]. CLBH calls for a pulse $\sim$ 10^{-11}–10^{-9} sec with contrast of the order of 10^6.

4. Since the cross-sectional area of the beam of the powerful laser must be large enough, owing to limitations imposed by the strength of the active elements, and also because of the specific features of the PF, it is necessary to focus the radiation in a number of experiments by a long-focus lens with $f = 10^2$ cm. This imposes rather stringent requirements on the divergence of the radiation, which must be not worse than 10^{-3} rad.

5. The PLR flux density should exceed all the thresholds of the basic parametric instabilities (see, e.g., the table in [16]). Furthermore, in the case of CLBH the target must be heated in the inertial-containment regime [17].

CHAPTER I

THE "FLORA" FACILITY

1. General Description of the "Flora" Facility

The diagram of the "Flora" facility is shown in Fig. 1. The facility consists of a high-power 20-channel neodymium-glass laser (see Fig. 2) and a "plasma focus." The light pulse in the laser part of the entire system is produced by specially designed generators.

The pulse from the generator is amplified with amplifiers arranged in series to an energy close to the self-focusing threshold. The pulse is then fed to a system where it is subdivided and subjected to series–parallel amplification, after which it enters the final ampli-
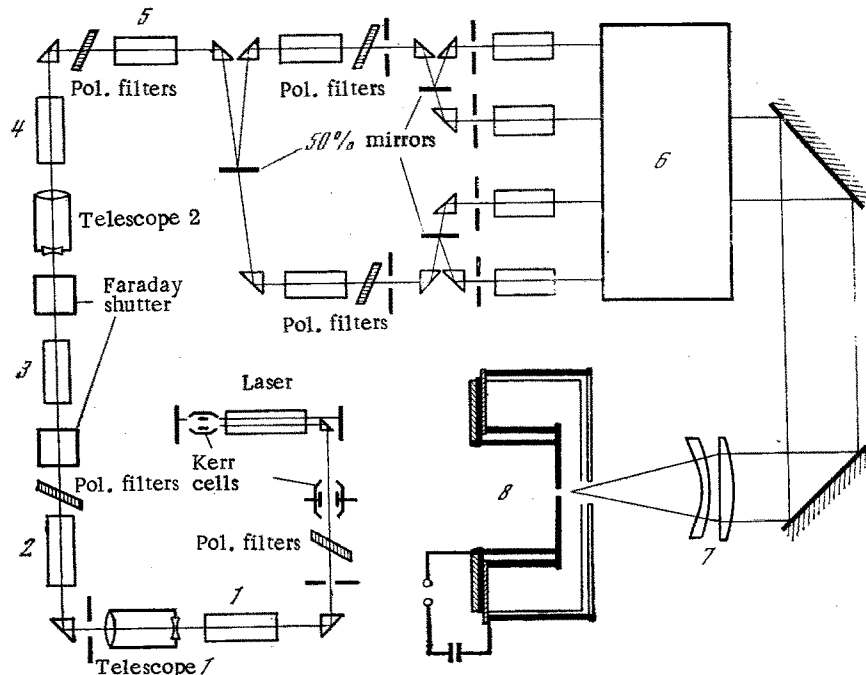

Fig. 1. Diagram of the "Flora" facility. 1-5) Preamplifiers; 6) 20-channel amplifier; 7) focusing objective; 8) "plasma focus."
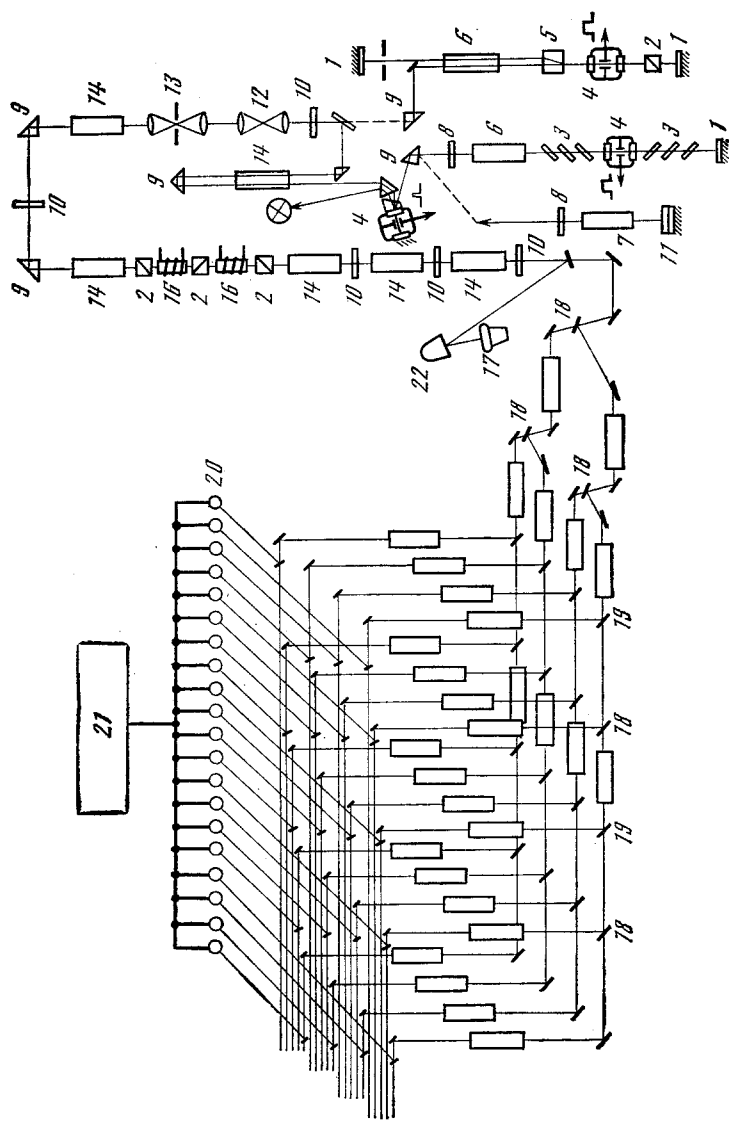
Fig. 2. Optical diagram of 20-channel laser. I) YAG-crystal mode-locking laser; II) laser with semiopen resonator; III) laser with two 100% mirrors; 1) 100% mirrors; 2) polarizers; 3) stacks; 4) Kerr cell; 5) beam splitter; 6) GLS-1 active element; 7) YAG active element; 8) 20% mirror; 9) prism; 10) saturable filters; 11) saturable filter combined with 100% mirror; 12) collimator; 13) collimator to protect against the reflected pulse; 14, 15) amplifiers; 16) Faraday shutter; 17) coaxial photocell; 18, 19) dividing elements; 20) calorimeter; 21) 20-channel calorimetric energy meter; 22) calorimeter.

163

fier stage, where 20 parallel beams of equal intensity (50 J in each beam) are formed. A focusing system focuses the laser radiation onto the target ("plasma focus"). The parameters of the "plasma focus" are: capacitor-bank energy 52 kJ, working voltage 27 kV, neutron yield $(2-4) \cdot 10^9$ neutrons/pulse.

2. The Driver Lasers

The main requirement imposed on the driver lasers of high-power multichannel laser installations is that they be reliable in operation and their time, energy, and spectral characteristics be stable. To develop a driver laser satisfying these conditions, we tried out a number of systems.

A. Laser with Two 100% Mirrors. The laser diagram is shown in Fig. 3. The Q-switching and the shaping of the short pulse are effected by a single electrooptical shutter located inside the resonator, which is made up of two flat 100% mirrors.

The distance between the mirrors is 1.4 m. Mode selection is by means of a diaphragm of 3-mm diameter. The active element (GLS-1 neodymium-glass rod of 20-mm diameter and 300-mm length) is placed in a GUS-1 four-lamp illuminator with cylindrical reflectors and IFP-8000 lamps. The pump energy is 10 kJ. The electrooptical shutter consists of a Kerr cell, a polarizer, and a polarizing beam splitter. The splitter separates the lasing channel from the channel through which the pulse is extracted from the laser. The polarizing beam splitters employed were a rhombic polarizer of calcite, a calcite cylinder cut at an angle to the optical axis, and crystalline quartz wedges (Fig. 4). The first two beam splitters can be easily adjusted and have a high transmission, $\sim 80\%$. However, the low endurance of calcite to the action of a powerful laser does not make it possible to use high radiation powers. A preferable beam splitter is therefore a wedge of crystalline quartz. The adjustment difficulties raised by dispersion can be circumvented by using the fact that the refractive index for the extraordinaey ray at $\lambda = 1.06$ µm is equal to the refractive index of the ordinary ray at $\lambda = 0.63$ µm. This makes is possible to use an He—Ne laser for the alignment.

The operating principle of the system consists in the following. When voltage is applied to the Kerr cell, the shutter opens and a Q-switching pulse is produced in the lasing channel. The voltage is then disconnected from the Kerr cell and part of the radiation accumulated in the resonator (in the gap between the left-hand mirror and the polarization beam splitter)
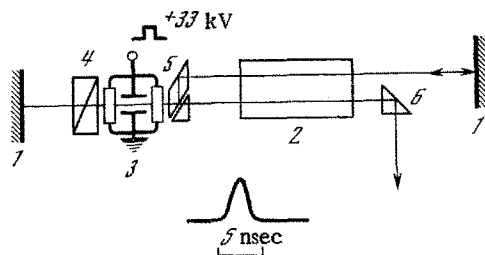

Fig. 3. Diagram of laser with two 100% mirrors. 1) 100% mirrors; 2) active element; 3) Kerr cell; 4) polarizer; 5) polarizing beam splitter.
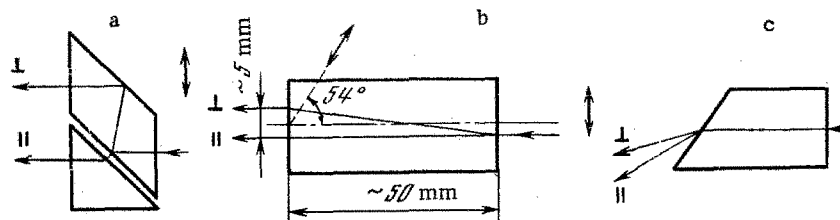

Fig. 4. Polarizing beam splitters. a) Rhombic calcite polarizer; b) calcite cylinder; c) crystalline-quartz wedge (the arrow denotes the direction of the optical axis of the crystal).
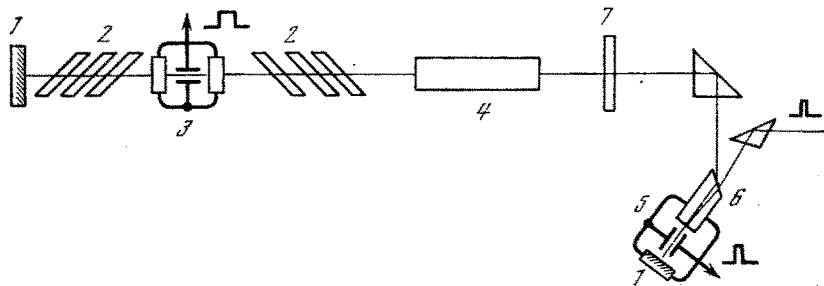
Fig. 5. Diagram of laser with semiopen resonator. 1) 100% mirrors; 2) stacks; 3, 5) Kerr cells; 4) active element; 6) quartz wedge; 7) 20% mirror.
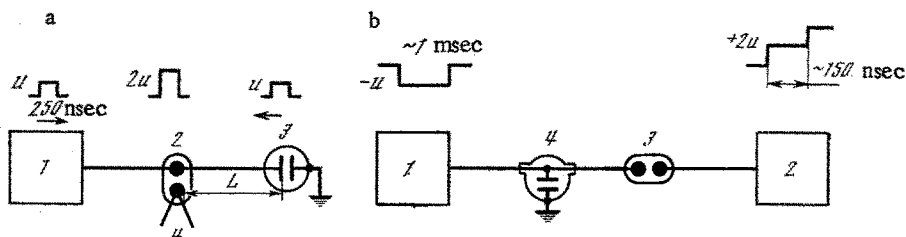

Fig. 6. Laser Q-control schemes. a) First variant; 1) modulator; 2) discharger; 3) Kerr cell; 4) long cable sections; b) second variant: 1) millisecond-pulse laser; 2) modulator; 3) discharger; 4) Kerr cell.

is extracted by the prism from the resonator. The pulse duration (τ_{pulse}) is determined by the duration (τ_f) of the voltage-dumping front and by the time ($2l/c$) of the travel of the radiation between the mirror and the polarization beam splitter:

$$\tau_{pulse} = 2(\tau_f + l/c). \qquad (1.1)$$

The short pulse passes through the active element of the laser, is amplified, and is directed by a turning prism to the input of the preamplification system. The corresponding pulse-cutout time diagram is shown in Fig. 7. The laser pulse duration is 70 nsec at the 0.1 level. The duration of the shortened pulse, measured with an I2-7 oscilloscope, was 3.9 nsec at the 0.1 level, with an output energy 0.1 J and a diffraction divergence $8 \cdot 10^{-4}$ rad.

The laser described above has a number of advantages over ordinary semiopen lasers with later shortening of the pulse [19]: it delivers at the output a much higher energy in a short pulse; it permits more reliable and stable synchronization; it makes use of only one Kerr cell, thereby decreasing substantially the energy loss; the presence of the amplification channel in the laser itself increases the efficiency of the latter, so that two preamplification stages can be eliminated. Finally, experience with a laser based on this scheme has shown that it is relatively simple to adjust and that it is most reliable. Some drawbacks of this scheme are the presence of quartz wedges in the resonator, which makes more stringent demands on the mechanical rigidity of the system elements and on the thermostatic control. In addition, the active element operates at a higher-radiation density, so that its useful lifetime is shortened. Therefore, in those cases when we needed a pulse of ordinary waveform we used a laser of standard design.

B. Laser with Semiopen Resonator. The diagram is shown in Fig. 5. The polarization elements were stacks of glass plates mounted at the Brewster angle; this made it possible to use less rigid mounts for these elements. The only adjustable elements were the mirrors. The short pulse was chopped with an electrooptical shutter consisting of a Kerr cell and a single crystalline-quartz wedge. Since the Kerr cells used in these two generators had the same electric parameters, the time characteristics of the two lasers were the same. The energy in the pulse was of the order of 2-3 MJ.

C. Kerr-Cell Voltage Supply Systems. The voltages were applied to the Kerr cells from one modulator [20] made up of coaxial cables and dischargers. Several variants of control
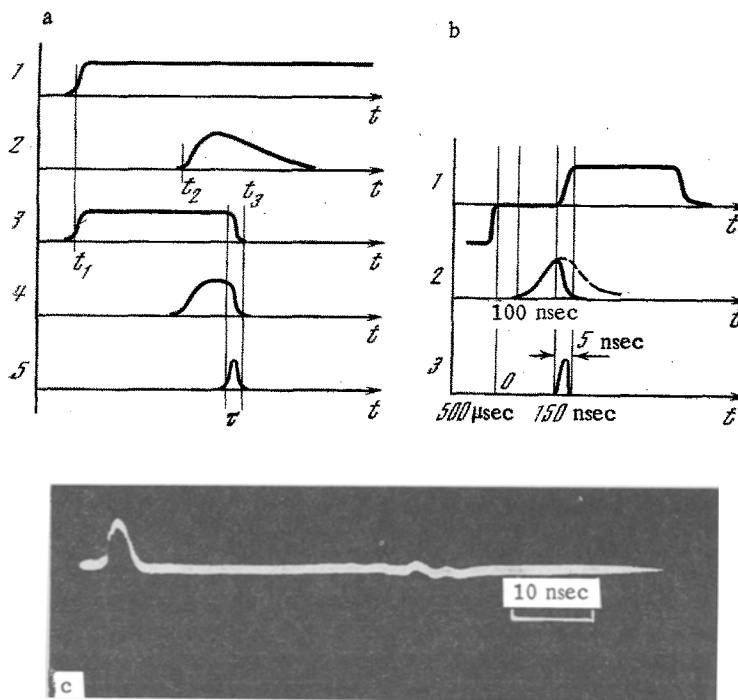
Fig. 7. Time diagrams of the lasers. a) First variant of Q control: 1) high-voltage pulse on Kerr cell without turning on discharger; 2) light pulse from laser under the condition No. 1; 3) voltage pulse on Kerr cell with the discharger connected; 4) light pulse in lasing channel under condition No. 3; 5) chopped "short" light pulse. b) Second variant of Q control: 1) high-voltage pulse on Kerr cell; 2) light pulse in lasing channel (the dashed curve shows the unshortened pulse); 3) shortened light pulse; c) oscillogram of short light pulse.

of the Q of the resonator were used. In the first variant, the Q was switched on when the voltage was applied and the short pulse was shaped when the voltage was removed from the Kerr cell; in the second variant, conversely, the Q switching was produced when the voltage was removed and the short pulse was shaped when it was applied. The first variant has a simple circuitry, but work with a laser having two 100% mirrors does not yield a sufficiently high radiation contrast. Better contrast is obtained with the second variant. Here, the circuit that controls the Kerr cell is somewhat more complicated. The circuits of the first and second variants are shown in Fig. 6. In the first circuit the pulse ($u = 16.5$ kV, $\tau = 250$ nsec) of the modulator passes through discharger 2 to the Kerr cell, is reflected from the cell and again returns to the discharger after a time $2L/v$ (where L is the length of the cable from the discharger to the cell and v is the velocity of pulse propagation in the cable). If the pulse duration exceeds $2L/v$, then the voltage at the electrode is doubled, the discharger, which is set for double the voltage, breaks down, and the voltage is removed from the cell after a time L/v.

We used also a system wherein the discharger was triggered by laser radiation. However, the operating stability was somewhat worse because the front of the triggering laser pulse was not steep enough. In addition, it was necessary to introduce into the resonator a plate to divert the radiation, and this caused deterioration of the resonator quality.

In the second scheme, the voltage is applied to the Kerr cell simultaneously with the triggering (the pulse parameters are: duration ~ 1 msec, voltage 16 kV). Then (after ~ 500 sec) a pulse with voltage -16 kV is applied to the Kerr cells and dumps its voltage. The time diagram of this laser scheme is shown in Fig. 7b.

3. Preamplification Stage

The laser output light pulse is directed to an amplification array (Fig. 2) consisting of six amplifiers connected in tandem in accordance with the standard scheme [8]. The active

elements of all the amplifiers are neodymium rods with dimensions 45 × 680 mm, placed in illuminators of the type GOS-1000B. This choice is dictated by the desire to standardize all the elements as much as possible. Each rod is pumped by four flash lamps IFP-20,000; the pump energy is 25 kJ. The end faces of the rods are cut at the Brewster angle.

The total gain in the working regime is of the order of 10^3; this makes it possible to raise the energy of the light pulse to 50 J at a duration 2 nsec at half-height and a divergence $2 \cdot 10^{-4}$ rad, and to 100 J at a divergence 10^{-3} rad at the self-focusing limit. On the other hand, in the case of a "long" pulse (~ 20 nsec) the energy can reach 150 J.

To prevent self-excitation and to decrease the background radiation, saturable dye-filled filtering cells are used in this system. For the same purpose, and also to suppress sharp peaks in the distribution of the energy over the beam cross section as a result of diffraction, aperture diaphragms were used, with diameters equal to the first diffraction minima at the amplifier outputs. The use of a system of special optical collimators has made it possible to obtain at the output of the amplifier line a divergence of $2 \cdot 10^{-4}$ rad. Measurements of the contrast of the radiation relative to the output energy have shown that in our case it is not worse than $5 \cdot 10^4$. The beam aperture at the output of the system is 43 mm.

4. Beam-Division Unit and Intermediate Amplification Systems

As indicated by various workers [82, 122], further amplification of the laser radiation to obtain high energies calls for an increase of the cross section of the light beam so as not to exceed the energy density capable of damaging the rods and the optical elements. There are two possibilities here. One is to increase directly the beam cross section, followed by amplification, e.g., with the aid of disk amplifiers [23]. The other calls for dividing the beam by optical methods, followed by series—parallel amplification [8, 22]. We used the latter method.

To this end, a beam-division system with series—parallel amplification was located ahead of the output power stage. We used three types of dividing elements: a) prisms operating near the total-internal-reflection angle [24]; b) plane-parallel plates of glass having a high refractive index [8]; c) mirrors with suitable reflection coefficients. Successive division into two and four beams in the horizontal plane was first used, after which each beam was divided into three and again into three in the vertical plane.

From the output of the amplifier array (Fig. 8) the radiation is fed to a prism that rotates the plane of polarization of the radiation through 90°, in view of the further need to subdivide the beam in the vertical plane with the aid of beam-splitting plates. The same element changes also the direction of the radiation by 90°. The division into two beams is effected with the aid of two right-angle prisms whose bases are mounted parallel to each other with a gap ~ 50 μm, and at an angle close to the total-internal-reflection angle. In this case the coefficient of Fresnel reflection from the surface increases sharply, and it is this which makes it possible, by suitable adjustment, to obtain effective division by practically any factor. We note that we use for the division two surfaces of two prisms, mounted with a high degree of parallelism and with a small gap in such a way as not to cause doubling of the focal spot or astigmatism of the passing beam. Inasmuch as in this case the reflection coefficients of both surfaces are comparable in magnitude, these surfaces constitute in effect a Fabry-Perot interferometer, to one of the fringes of which the dividing element is in fact adjusted. The band is chosen in the course of the adjustment in such a way that the reflected and transmitted beams are of equal intensity and that the radiation be as uniform as possible over the beam cross section. The energy loss on the surfaces of the optical elements that guide the radiation amounted in this case to 25%. Thus, after division into two, the energy of each beam was 37% of the energy at the exit from the preamplification system.

The two beams were then fed to intermediate amplifiers, where they were amplified to an energy of the order of the energy at the output of the preamplification stage, after which each of the beams was again divided into two, in the manner described above. The four beams obtained as a result of the division were amplified by four parallel amplifiers whose gains made it possible to compensate for the energy losses in the optical elements of the division system and to obtain in each of the beams an energy of the order of the beam energy prior to the division.

Each of the amplified four beams enters a system that divides it into three (Fig. 9). Division into three is effected in the vertical plane either by two beam-splitting plates
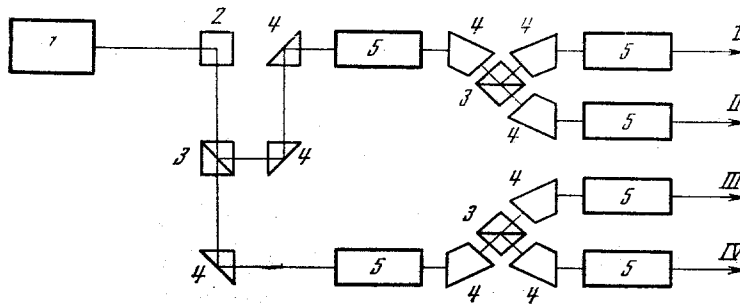
Fig. 8. Diagram of beam division into four. 1) Pre-amplification stage; 2) prism that rotates the plane of polarization through 90°; 3) dividing prisms (or mirrors); 4) intermediate amplifiers. The Roman numerals denote the numbers of the channels.
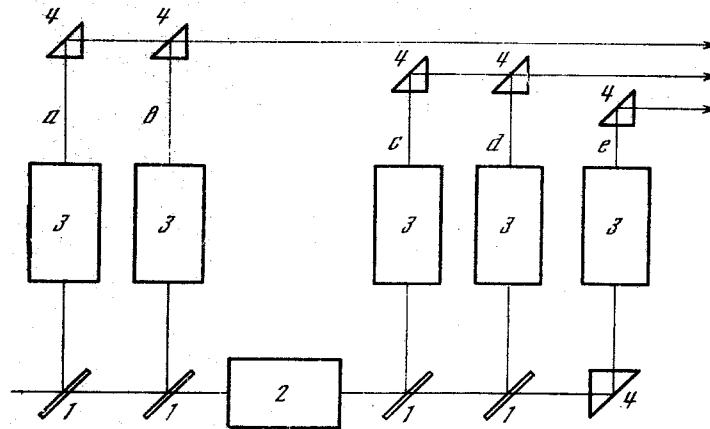

Fig. 9. Scheme for division and parallel–series amplification in the final stage of one of the four beams obtained after division into four (see Fig. 8). 1) Beam splitting plates or dielectric-coated mirrors; 2) intermediate amplifier; 3) final amplification stages; 4) rotary prisms. The Latin letters number the channels.

of glass with high refractive index, mounted at an angle of 45° to the beam axis [8], relative to the incident energy or else by mirrors with dielectric coatings. In the former case the energy balance relative to the incident energy is the following: $\simeq32\%$ in the first reflected beam, $\simeq23\%$ in the second, and $\simeq45\%$ in the transmitted beam. The shortcomings of the division with plane-parallel plates are the following: a) the need for high precision in the preparation of the plates, since the interference fringes must be wider than the beam diameter; b) the associated difficulty of mounting these plates, since the smallest bending of the surfaces gives rise to interference fringes; c) the beams resulting from the division are not of equal intensity; d) this scheme gives rise to the effect of "fragmentation" of the focal spot, which was discussed in [8].

More convenient is division with the aid of mirrors with dielectric coatings, which are resistant to intense laser radiation. The first mirror in the beam path has a reflection coefficient 30%, and the remaining ones 50%. Thus, the light beam breaks up into three beams of equal intensity. The beams reflected from the mirrors enter the final amplification stages with an amplification factor k = 3, are amplified again to the initial energy, and are again divided into three by the method described above. In principle, this division can be continued to infinity. In the present installation, we confined ourselves to a second division into three, obtaining as a result 20 beams of equal intensity.

It should be noted that this system of division has practically complete τ synchronism (determined only by the accuracy with which the optical elements are manufactured), without the use of any compensating devices such as optical delays [21]. In addition, since the pre-

amplification stage and the division system do not play an important role in the energetics of the laser, we used weaker pumping in these elements, making it possible to maintain the radiation divergence at a high level. We point out also the relative simplicity of adjusting the division system, which can be effected with light from an He—Ne laser, since all the optical elements used by us can cause only a negligible parallel shift of the beam on account of the dispersion of the glass.

5. 20-Channel Amplifier and Formation of the Output PLR

The 20-channel amplifier was structurally assembled in a rack with vertically suspended illuminators of the GOS-1001 type. The dimensions of the complete final stage, including the system for division into three and for shaping the output beam are: length of rack 2800 mm, width 700 mm, height 1500 mm. Each illuminator contains four IFP-20,000 lamps fed from a capacitor bank. The pump energy is ~ 10 kJ per lamp, and the pump flash duration is ~ 1 msec. Each illuminator pumps a rod measuring 630×45 mm with end faces cut at an angle of $85°$. The gain of each channel is $k = 3$. The maximum total energy of all the beams is $E \simeq 1000$ J in a pulse of duration 2 nsec at half-height, and above 2000 J in a pulse of 20 nsec at half-height, at a divergence on the order of $3 \cdot 10^{-4}$ rad. The output beam is shaped with the aid of a system of rotary prisms. Inclining the vertical illuminators and a corresponding arrangement of the prisms (Fig. 2) produces in a horizontal direction a beam assembly consisting of 20 beams placed flush against each other, as shown in Fig. 10, and inscribed in a circle of ≈ 260-mm diameter.

All the amplifiers, dividing elements, and rotary prisms, which carry the radiation, are so arranged that the optical lengths of all 20 channels are automatically equal, without any optical additional elements, and produce a minimal focal spot.

6. Parameters of the Radiation at the Output of the Laser

The radiation energy, the pulse waveform, the divergence, and the spectral composition were monitored at different points of the facility: at the output of the driver laser, at the output of the preamplification system, after the division into two and into four, and at the output of the entire system.

The corresponding values of the energy, at a divergence $3 \cdot 10^{-4}$ rad, are listed below, where τ is the duration of the light pulse; E_{dl}, energy of the driver laser; E_{pa}, energy at the preamplification system; E_1, energy after division into two; E_2, energy after division into four; E_3, total energy at the output of the system; Q_1, maximum flux density of the laser radiation at a divergence $2\alpha = 3 \cdot 10^{-4}$ in the case when the beams are focused by individual lenses; Q_2, maximum flux density of the given laser in the case when the composite beam is focused by a single lens; B, brightness of the radiation at the laser output calculated over the areas of the beams:

τ, nsec	E_{dl}, J	E_{pa}, J	E_1, J	E_2, J	E_3, J	Q_1, W/cm²	Q_2, W/cm²	B, W/cm²·sr
2	0,1	50	96	190	960	$9,6 \cdot 10^{15}$	$4 \cdot 10^{14}$	$2,2 \cdot 10^{15}$
20	0,5	110	270	460	2120	$2,1 \cdot 10^{15}$	$9 \cdot 10^{13}$	$5,1 \cdot 10^{14}$

The laser energy was measured with the aid of a 20-channel calorimetric module prepared by the All-Union Scientific-Research Institute for Optical Physical Measurements (VNIIOFI). A block diagram of the module is shown in Fig. 11. All the calorimeters were calibrated at the VNIIOFI against the "Laser Test Installation No. 1 for Energy-Measuring Devices."
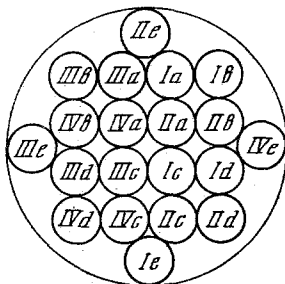

Fig. 10. Arrangement of beams in the plane of the focusing lens (viewed from the target). The numbers of the channels correspond to the notation of Figs. 8 and 9. The diameter of the circumscribed circle is 260 mm.
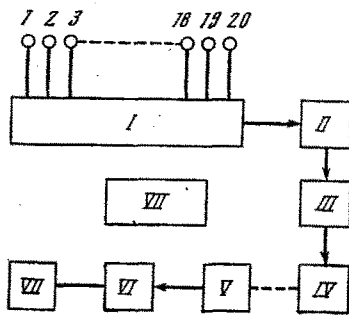
Fig. 11. 20-channel calorimetric energy meter.
I) Calorimeters; II) digital voltmeter; III)
control block; IV) tape perforator; V) optical
sensing unit; VI) transcriptor; VII) digit prin-
ter; VIII) power pack.

Fig. 12. Oscillogram of 20-nsec pulse past
the driver laser (a) and at the exit from
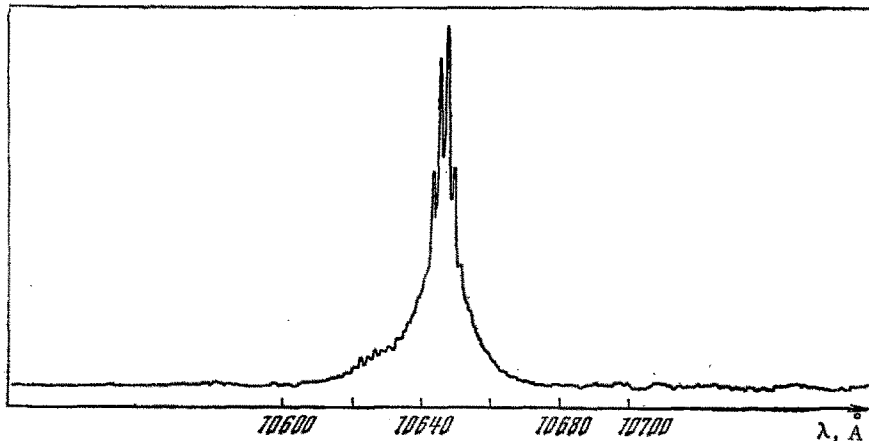one of the power amplifier channels (b).

Fig. 13. Emission spectrum of generator with two 100%
mirrors.

Measurements of the pulse waveform have shown that in the case of the short pulse (~ 2
nsec) its waveform and duration are not altered substantially as the pulse moves through the
amplifier stages. As to the 20-nsec pulse, its waveform is substantially distorted. Whereas
at the output of the driver laser the shape is close to trapezoidal, at the output of the
final stages its leading front becomes steeper and the trailing edge is stretched out (Fig.
12).

Measurements were made of the spectral composition of the laser radiation at the output
of the driver laser and at the output of the preamplification stage. Figure 13 shows the
emission spectrum of the driver laser with two 100% mirrors. As seen from the figure, the
emission spectrum consists of three narrow lines separated by 1.8 Å. The reason is that the
resonator of this laser contained a plane-parallel plate 1.8-mm thick, which caused mode dis-
crimination.

Figure 14 shows the change of the emission spectrum of the driver laser with semiopen
resonator as a function of the pump. It is seen that the spectrum broadens with increasing
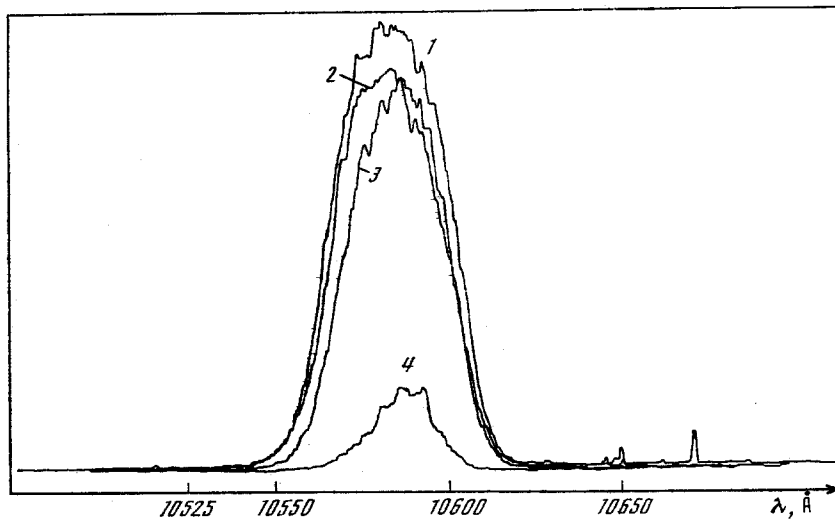pump.

170

Fig. 14. Spectral composition of emission of generator with
semiopen resonator as a function of the pump. 1) Spectrum
at a pump 18.8 kJ; 2) 17.8 kJ; 3) 16.4 kJ; 4) 15.1 kJ.

The mission spectrum at the output of the preamplification stage is somewhat broader
than at the generator output (Fig. 15). In addition, an absolute wavelength calibration was
made against the spectrum of the sun (Fig. 15).

Measurements of the radiation divergence were made at the outputs of the driver laser,
of the preamplification stage, and in the composite beam at the output of the entire system.
Figure 16 shows the measurement results.

The contrast of the radiation of the laser installation was measured with a calorimeter
in control flashes without shortening the pulse, and amounted to not less than 10^5.

Depending on the purpose and specific features of the experiment, several focusing vari-
ants can be used for the radiation: 1) with the aid of small-diameter lenses placed in each
beam, so as to illuminate the target from all directions; 2) by a single lens of 300-mm diam-
eter and focal length f = 150 cm; 3) with the aid of a two-lens objective.

The lenses and the two-lens objective were designed for minimal spherical aberrations
and in such a way that the radiation reflected from the second lens was not focused into the
first lens. The radiation flux densities at the target, obtained by focusing with the aid
of these systems, were given above.

In the case when aspherical optics are used, the dimension of the focal spot can be de-
creased to values of the order of 20-30 μm [25]. The maximum attainable laser-radiation
laser flux is then of the order of 10^{17} W/cm^2.

7. Monitoring the Laser Parameters

To check on the space—time characteristics of the laser radiation, a pulse from the pre-
amplifier was focused on an aluminum target. The power flux at the target reached in this
case $9 \cdot 10^{12}$ W/cm^2. Spectra of hydrogenlike and heliumlike aluminum were obtained (Fig. 17)
in the range 5.6-7.8 Å in the first and second orders of reflection from the crystal. An
x-ray spectrograph was used with a convex mica crystal [26, 27], which made it possible to
obtain spectra in the range 1.5-19.5 Å.

The plasma density was determined from the ratio of the intensities of the intercombina-
tion and resonance lines of Al XII [28]:

$$\alpha = \frac{I_I}{I_R} = \alpha_0 + N_e \left[(\alpha_0 + 1)\, C\,(2^3;\, 2^1) + \alpha_0 C\,(2^3;\, i) \right] [0,25 A\,(2^3 P_1;\, 1^1 S_0)]^{-1},$$

where

$$\alpha_0 = [C\,(1^1 S_0;\, 2^1 S_0) + C\,(1^1 S_0;\, 2' P_1)] \left[C\,(1^1 S_0;\, 2^3 S_1) + \sum_{j=0}^{2} C\,(1^1 S_0;\, 2^3 P_j) \right]^{-1},$$

171

A(k, l) is the probability of the radiative transition k → l; C (i, j) = N_eV [$v\sigma$(i → j)] is the rate of the i → j transition on account of electron—ion collisions.

The plasma temperature was determined from the ratio of the intensities of the dielectronic satellites to the resonance line of Al XII [29]:

$$i_s^d = \frac{I_s^d}{I_R} = 1.5 \cdot 10^{-15} \frac{g_s}{g_0} \frac{A_a}{B} \frac{A_r}{A_a + \sum A_r} \frac{|E_0|}{kT_e} \exp(|E_0|/n^2 kT_e),$$

where g_s and g_0 are the statistical weights of the autoionization level and of the level to which the transition takes place; n, principal quantum number; A_a and A_r, probabilities of the autoionization and radiative decays; B, a parameter that depends on the type of transition; E_0, energy of the autoionization level, reckoned from the boundary of the continuous spectrum.

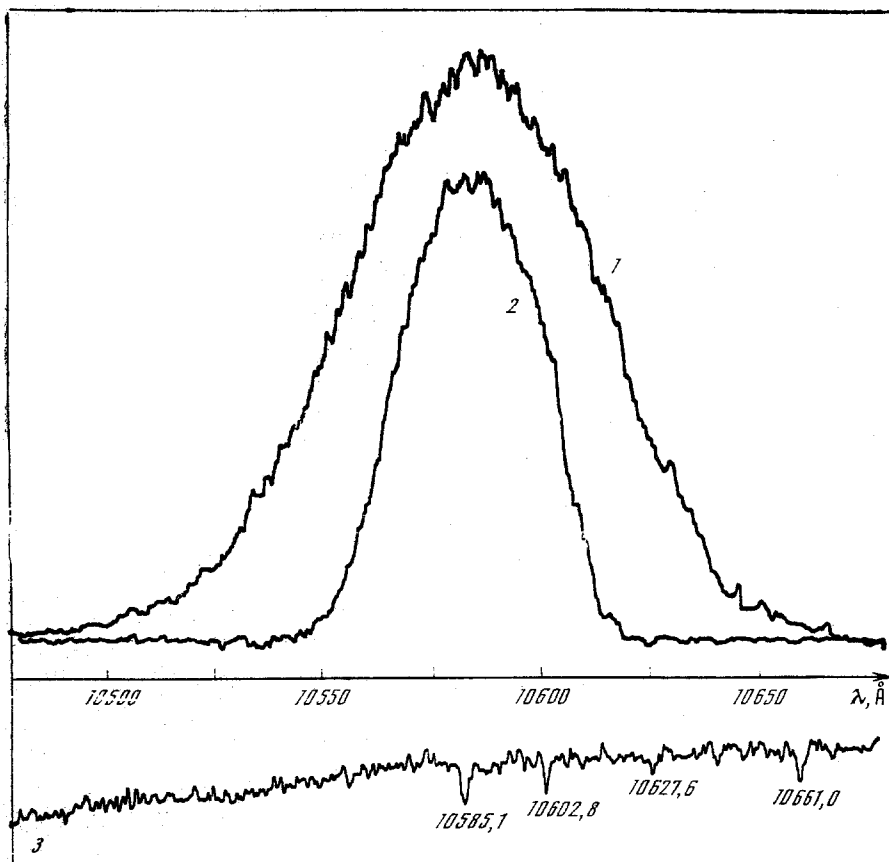

Fig. 15. Spectral composition at the outputs of the preamplification stage and of the driver laser. 1) Preamplification spectrum; 2) driver-laser spectrum; 3) spectrum of the sun.
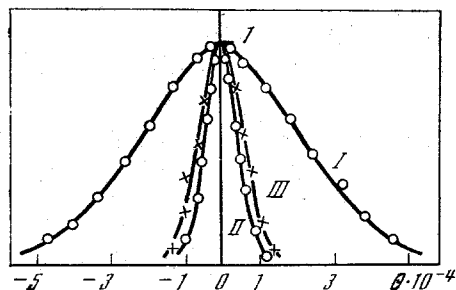

Fig. 16. Dependence of the relative intensity of the radiation on the angle: I) at the output of the driver laser; II) at the output of the preamplification stage; III) at the output of the complete laser system.
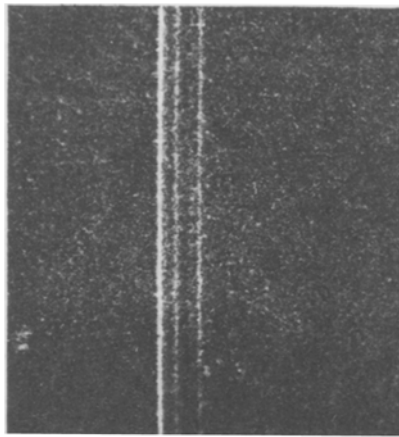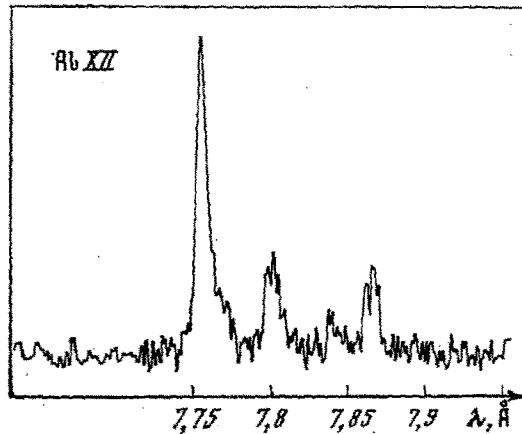
Fig. 17. Spectrum of hel-
iumlike Al XII.

Fig. 18. Photographic density patterns
of the spectra of hydrogenlike and heli-
umlike Al XII.

The reduction of the photographic density patterns of the obtained spectra (Fig. 18) has shown that the parameters the aluminum plasma produce at such fluxes ($T_e \approx 200$ eV; $N_e \approx 10^{20}$ cm^{-3}) agree with the plasma parameters obtained in other installations at analogous laser-radiation fluxes [30].

The contrast of the laser radiation was checked by an interferometry procedure. To this end, the radiation of the laser, with the pulse-shortening system turned off, was focused on an aluminum target. A Mach-Zehnder interferometer with auxiliary illumination by a ruby laser was used for the diagnostics. The duration of the ruby-laser pulse was 1.4 nsec at half-height.

In none of the monitoring flashes were deviations of the interference fringes observed. Recognizing that the sublimation of the matter takes place at a radiation flux density not less than 10^7-10^8 W/cm^2, we can state that the contrast in our case (see table p. 169) is worse than 10^7 in power and 10^6 in energy.

CHAPTER II

COMBINED LASER AND BEAM PLASMA HEATING

1. Combined Laser and Beam Heating

It is of interest to compare the data on the relaxation length of the beam in a plasma obtained in installations of the Z-pinch type (Z-pinch, "plasma focus," vacuum spark, etc.) (see Fig. 19). Experiment shows [11, 31] that during the initial instant after its forma-tion, the beam passes unobstructed through the plasma (the deceleration length is classical).

Only after self-focusing of the beam in the plasma and after heating of the latter by the turn current to temperatures on the order of several kiloelectronvolts does the relaxation, length shorten radically. It follows from the estimates [5, 32] that for the development of collective processes in a plasma with a solid-body density $n_e \sim 10^{23}$ cm^{-3} the required electron temperature is of the order of 1 keV. As indicated in the introduction, such a temperature is presently practically impossible to attain by heating with the backward current. This is the first among many causes that prompt the use of lasers to prepare the target for interaction with the powerful electron beam. Extrapolation of the data of Fig. 19 into the region of densities of the order of those of solids shows that one can count in this case on a relaxation length of the order of 10^{-3}-10^{-4} cm in solid deuterium, which is larger by one order of magnitude than the value obtained from the growth rate of two-stream instability, and is smaller by two or three orders of magnitude than the classical deceleration length.

A second benefit ensuring from the use of the laser to "prepare" the target is the possiblity of producing the necessary [5, 32] density gradient. A third cause is the possibility of focusing the REB in the plasma produced by the laser [6, 7]. In addition, as will be shown later on, powerful laser radiation acting in the plasma together with an REB can produce a number of effects that improve, from the point of view of obtaining high temperatures and densities, both the processes of the absorption of the REB and of the plasma heating, and the gasdynamic processes in cumulative target compression. For example, it is possible to decrease the danger of heating the core of the target by the fast electrons and to change the character of the transport processes, thereby relaxing the requirements on the energetics of the system, and others.

Among the advantages of laser energy sources are the relative ease of focusing the beam on the target, the high rate of energy input into the medium (typical values of radiation flux of high-power neodymium-glass and CO_2 lasers reach at the present time values of the order of 10^{14}-10^{17} W/cm^2 [18, 22]), the high coefficient of absorption of the laser radiation in the target [3, 33, 34], the fact that the photon has no charge, and the feasibility in principle of obtaining for a spherical target a compression coefficient of the order of 10^3 [33]. At the same time, the presently employed lasers have relatively low efficiencies.

The low optical breakdown strength of the optical elements and the danger of laser self-excitation make it necessary to employ multimodule systems with decouplers, making the installation less reliable and more expensive. In addition, the large number of optical elements in the laser, which are manufactured with finite precision, imposes certain limitations on the radiation parameters. The energy of the presently produced lasers amounts to 10^4 J.

On the other hand, the presently available REB accelerators have energies of the order of 10^5-10^6 J and a high efficiency. In addition, inasmuch as a magnetic field is always associated with an electron beam, there are hopes of producing in the target magnetized thermal conductivity [6, 7, 35]. However, the difficulties involved in focusing and in obtaining short REB pulses of high energy decrease the value of the energy flux to the target to an order of 10^{13} W/cm^2 [7] and decrease the efficiency of the accelerator. The use for using multimodule systems adds also problems of synchronizing the individual modules. In addition, the low efficiency of the classical absorption of electrons even in heavy shells, on the one hand, and the difficulty of exciting collective processes in a cold solid target, on the other, as well as the maximum theoretical value of the attainable compression of a solid target, 10^2 [6], greatly increase the energy that an REB accelerator must deliver to produce controlled thermonuclear fusion, compared with laser systems.

Despite the fact that work is presently being done on the improvement of both laser-driven and beam systems, it is clear that to decrease the requirements with respect to the energetics of the system of the target used for the heating and to increase its efficiency it would be desirable to use a heating method that incorporates the better features of REB and PLR sources.

In connection with the foregoing, we regard the realization of combined laser-and-beam heating of a plasma as quite promising. The principal role in the energetics of such a facility should be played by the REB, which can be obtained with high efficiency. In addition, from a comparative analysis of installations of the Z-pinch type [11] it is seen that decreasing the pinch diameter (at least to certain limits) increases the energy of the electrons of the beam produced after the current is interrupted.

Next, to produce an optimal system (energy source + target), which provides an optimal gain $k = E_{thermon}/E_{cor}$, the following must be done: 1) use spherical or cylindrical targets;
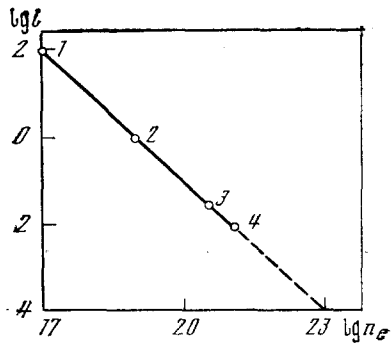
Fig. 19. Data on the the relaxation length of an electron beam in a plasma.

2) ensure in the final state of the medium with the high temperature an average DT-mixture density of the order of 10^2-10^3 g/cm^3; 3) ensure a maximum absorption of the source energy in the corona and a maximum transfer of the energy from the corona to the "pusher," $\eta = E_{kin}/E_{cor}$; 4) shape definite density and temperature profiles in the course of the cumulative compression of the target, by shaping the pulse from the energy source or by special construction of the target; it is necessary in this case to attempt to work with targets of large DT mass ($\geqslant 10^{-2}$ g for $E_0 \lessgtr 10^6$ J); 5) choose the target construction and its heating conditions in such a way as to reduce to a minimum the influence of the hydrodynamic instability on the cumulative process.

To ensure absorption of the REB in the target by collective processes, it is necessary to deposit on the surface of the target a layer of thickness of the order of 10^{-3}-10^{-4} cm in such a way that this zone constitutes a plasma with temperature higher than or of the order of 1 keV. To decrease the stabilizing influence of the plasma density gradient [36] on the Langmuir noise, this gradient should be eliminated if possible These conditions can be satisfied by heating the target with the laser alone prior to the combined heating, provided that the preliminary laser heating is produced in the thermal-wave regime. We confine ourselves to consideration of a planar geometry of the heating process, which can be treated analytically. The solution of the corresponding thermal problem [37] in the planar case yields the following expressions for the required duration τ_0 of the laser pulse and for the laser radiation energy density $q_0 \tau_0$:

$$\tau_0 \simeq 1.2 \cdot 10^{-29} Z^2 \Lambda \; x_0^2 T_0^{-5/2}, \tag{2.1}$$

$$q_0 \tau_0 \simeq 2.5 \cdot 10^{-9} Z n_0 x_0 T_0, \tag{2.2}$$

which are valid under the condition

$$\tau_0 \leqslant \tau_{ei} = \frac{10^{13} A T_0^{3/2}}{Z^3 \Lambda n_0}, \tag{2.3}$$

where x_0 is the depth of the solid-target zone heated by the thermal wave; Λ, Coulomb logarithm; q_0, laser radiation flux density in W/cm^2; A, atomic weight of the target material; T_0, temperature, n_0, density; and Z, charge.

It is easy to obtain from these relations that in the case of a DT target with density $n_0 = 5 \cdot 10^{22}$ cm^{-3} a temperature $T_0 = 1$ keV can be reached in a layer of thickness $x_0 = 10^{-3}$ cm at $\tau_0 \simeq 10^{-11}$ sec and $q_0 \tau_0 \simeq 10^4$ J/cm^2. In the case of a CD_2 target, a temperature of 2 keV can be obtained at the same layer thickness with $\tau_0 \simeq 10^{-10}$ sec and $q_0 \tau_0 \simeq 10^5$ J/cm^2.

The laser described above is capable of ensuring preliminary heating of the target in the indicated regime.

It will be shown in Sec. 4 of Chap. II that the indispensable condition for producing a high-power neutron is the use of solid targets of special construction. It is necessary in this connection to consider the process of CLBH of the plasma at densities close to the critical value for laser radiation. Since the target is located inside the pinch and the current sheath will interact with this target, it is necessary to consider also the influence of the current on the CLBH mechanisms.

An important problem is to ensure maximum absorption of the REB and PLR energy when they interact jointly with the plasma. The next two sections (Secs. 2 and 3) are devoted to a

175

theoretical consideration of those aspects of this problem, and the possible causes of the increase absorption of energy by the plasma due to the development of instabilities and turbulence in the plasma.

In Sec. 2 we obtain on the basis of the linear theory the growth rates and the thresholds of the instability that is produced when laser radiation and an electron beam interact with a current plasma in the critical-density region. It is shown that the beam and the current can significantly lower the threshold of the parametric instability that contributes to the anomalous absorption of the laser energy. On the other hand, a relatively weak field lowers the threshold of excitation of the Langmuir turbulence by the electron beam, a fact that likewise contributes to a more effective absorption of the beam energy in the plasma.

In Sec. 3 are given nonlinear estimates of the effective collision frequency, which characterizes the rate of turbulent absorption of laser energy by the plasma. This collision frequency depends substantially on the beam parameters and under definite conditions it can greatly exceed the frequency of the Coulomb collision even if electromagnetic radiation of the laser is relatively weak and does not excite any parametric instability in the absence of an electron beam.

2. Combined Interaction of Laser and Electron Beams with the Target Plasma. Kinetic Instabilities

In this section we consider the instabilities that are produced in combined interaction of an electron beam and a pump wave with a current plasma. The dispersion equation for longitudinal perturbations of a plasma acted upon by high-power pump wave

$$E(t) = E_0 \sin \omega_0 t \tag{2.4}$$

with frequency ω_0 and electric field intensity vector E_0, takes the form (see Eq. (7.3) in [14])

$$\frac{1 + \delta\varepsilon_e(\omega, k) + \delta\varepsilon_i(\omega, k)}{[1 + \delta\varepsilon_e(\omega, k)]\,\delta\varepsilon_i(\omega, k)} + \frac{(kr_E)^2}{4}\left[\frac{1}{\varepsilon(\omega + \omega_0, k)} + \frac{1}{\varepsilon(\omega - \omega_0, k)}\right] = 0. \tag{2.5}$$

Here $r_E = eE_0m^{-1}\omega_0^{-2}$ is the oscillation amplitude of an electron (with charge e and mass m) in a low-frequency electric field (2.4), $|kr_E| \ll 1$; $\delta\varepsilon_{e,i}(\omega, k)$ is the contribution of the electrons (or of ions with charge e_i) to the longitudinal dielectric constant by the plasma oscillations of frequency ω and wave vector k:

$$\varepsilon(\omega, k) = 1 + \delta\varepsilon_e(\omega, k) + \delta\varepsilon_i(\omega, k).$$

We consider a plasma (with electron density n_e and temperature T_e) through which an electron current flows with a current velocity u.

In addition, in the same direction as the current, there passes through the plasma a beam of electrons with density $n_b \ll n_e$, temperature T_b, and velocity u_b; $[uu_b] = 0$, $(uu_b) > 0$, $u_b \gg u$.

We assume that the pump frequency ω_0 is close to the plasma frequency:

$$|\omega_0 - \omega_p| \ll \omega_p, \tag{2.6}$$

where

$$\omega_p = (\omega_{L_e}^2 + \omega_{L_i}^2)^{1/2}, \qquad \omega_{L_{e,i}} = (4\pi e^2 n_{e,i}/m_{e,i})^{1/2}.$$

Under the conditions (2.6) it is possible to have in the plasma an instability connected with the decay of the pump wave into a high-frequency Langmuir wave $(\omega_{L_e} \sim \omega_0 \gg kv_{T_e})$ and a low-frequency wave $(\omega \ll kv_{T_e})$. We study the influence of the electron beam and of the current on this instability. Assuming that the phase velocity of the low-frequency oscillations is located between the thermal velocities of the electrons and ions:

$$v_{T_i} \ll \frac{\omega - ku}{k} \ll v_{T_e}, \tag{2.7}$$

and that the beam velocity is high enough:

$$u_b \sim c, \quad |ku_b| \gg kv_{T_b}, \omega; \quad |\omega \pm ku_b| \gg kv_{T_b}, \omega \tag{2.8}$$

we obtain for the partial contributions of the ions and electrons of the plasma and of the beam to the longitudinal dielectric constant the following expressions:

$$\delta\varepsilon_i(\omega, \mathbf{k}) = -\frac{\omega_{L_i}^2}{\omega^2}\left[1 - i\sqrt{\frac{\pi}{2}}\frac{\omega^3}{k^3 v_{T_i}^3}\exp\left(-\frac{\omega^2}{2k^2 v_{T_i}^2}\right)\right], \tag{2.9}$$

$$\delta\varepsilon_i(\omega \pm \omega_0, \mathbf{k}) = -\frac{\omega_{L_i}^2}{\omega_0^2}, \tag{2.10}$$

$$\delta\varepsilon_e(\omega - \mathbf{ku}, \mathbf{k}) = \frac{1}{k^2 r_{D_e}^2}\left[1 + i\sqrt{\frac{\pi}{2}}\frac{\omega - \mathbf{ku}}{k v_{T_e}}\right], \tag{2.11}$$

$$\delta\varepsilon_e(\omega - \mathbf{ku} \pm \omega_0, \mathbf{k}) = -\frac{\omega_{L_e}^2}{\omega_0^2}\left[1 + \frac{3k^2 v_{T_e}^2}{\omega_0^2} \mp \frac{2(\omega - \mathbf{ku})}{\omega_0} \mp i\sqrt{\frac{\pi}{2}}\frac{\omega_0^3}{k^3 v_{T_e}^3}\exp\left(-\frac{\omega_0^2}{2k^2 v_{T_e}^2}\right) \mp i\frac{\nu_{ei}}{\omega_0}\right], \tag{2.12}$$

$$\delta\varepsilon_b(\omega - \mathbf{ku}_b, \mathbf{k}) = -\frac{\omega_{L_b}^2}{(\omega - \mathbf{ku}_b)^2}\sqrt{1 - u_b^2/c_2}\left[1 - \frac{(\mathbf{ku}_b)^2}{k^2 c^2}\right] + i\sqrt{\frac{\pi}{2}}\frac{(\omega - \mathbf{ku}_b)(1 - \omega^2/k^2 c^2)}{k'^3 r_{D_b}^3 \omega_{L_b}(1 - u_b^2/c^2)}\frac{(\mathbf{ku}_b)^2}{\omega^2}\exp\left(-\frac{\omega'^2}{2k'^2 v_{T_b}^2}\right), \tag{2.13}$$

$$\delta\varepsilon_b(\omega - \mathbf{ku}_b \pm \omega_0, \mathbf{k}) = -\frac{\omega_{L_b}^2}{(\omega_0 \mp \mathbf{ku}_b)^2}\sqrt{1 - u_b^2/c^2}\left[1 - \frac{(\mathbf{ku}_b)^2}{k^2 c^2}\right]$$

$$\pm i\sqrt{\frac{\pi}{2}}\frac{(\omega_0 \mp \mathbf{ku}_b)(1 - \omega_0^2/k^2 c^2)}{k'^3 r_{D_b}^3 \omega_{L_b}(1 - u_b^2/c^2)}\frac{(\mathbf{ku}_b)^2}{\omega_0^2}\exp\left(-\frac{(\omega_0 \mp \mathbf{ku}_b)^2}{2k'^2 v_{T_b}^2(1 - u_b^2/c^2)}\right), \tag{2.14}$$

where ω' and $\mathbf{k}'$ are the Lorentz-transformed frequency and wave vector [38]:

$$\omega' = \frac{\omega - \mathbf{ku}_b}{\sqrt{1 - u_b^2/c^2}}, \tag{2.15}$$

$$\mathbf{k}' = \mathbf{k} + \mathbf{u}_b \frac{\mathbf{ku}_b\left(1 - \sqrt{1 - u_b^2/c^2}\right) - \omega u_b^2/c^2}{u_b^2 \sqrt{1 - u_b^2/c^2}}. \tag{2.16}$$

Substituting expressions (2.9)-(2.14) in the dispersion equation (2.5) and introducing the notation

$$\sqrt{\frac{\pi}{8}}\frac{(\omega - \mathbf{ku})\omega}{k v_{T_e}} - \sqrt{\frac{\pi}{8}}\frac{(\mathbf{ku}_b)^3 k^3 r_{D_e}^3 (1 - \omega^2/k^2 c^2)}{\omega_{L_b} k'^3 r_{D_b}^3 \omega (1 - u_b^2/c^2)}\exp\left(-\frac{(\mathbf{ku}_b)^2}{2k'^2 v_{T_b}^2(1 - u_b^2/c^2)}\right) \equiv \gamma_s \tag{2.17}$$

for the low-frequency "damping decrement" and

$$\frac{\nu_{ei}}{2} + \sqrt{\frac{\pi}{8}}\frac{\omega_{L_e}}{k^3 r_{D_e}^3}\exp\left(-\frac{\omega_{L_e}^2}{2k^2 v_{T_e}^2}\right) + \sqrt{\frac{\pi}{8}}\frac{\omega_{L_e}(\omega_{L_e} \pm \mathbf{ku}_b)}{\omega_{L_b} k'^3 r_{D_b}^3 (1 - u_b^2/c^2)}\left[1 - \frac{\omega_0^2}{k^2 c^2}\right]\frac{(\mathbf{ku}_b)^2}{\omega_0^2}\exp\left(-\frac{(\omega_0 \pm \mathbf{ku}_b)^2}{2k'^2 v_{T_b}^2(1 - u_b^2/c^2)}\right) \equiv \tilde{\gamma}_\pm \tag{2.18}$$

for the high-frequency "damping decrement," we obtain an equation for the frequency and for the growth rate

$$\omega^2 - k^2 v_s^2\left\{1 + \frac{(\mathbf{kr}_E)^2}{8k^2 r_{D_e}^2}\omega_0 \mathrm{Re}\left[\frac{1}{\Delta\omega_0 + \omega - \mathbf{ku} + i(\gamma + \tilde{\gamma}_-)} + \frac{1}{\Delta\omega_0 - (\omega - \mathbf{ku}) - i(\gamma + \tilde{\gamma}_+)}\right]\right\} = 0, \tag{2.19}$$

$$i(\gamma + \gamma_s) - \frac{(\mathbf{kr}_E)^2}{16k^2 r_{D_e}^2}\omega_0 k v_s \mathrm{Im}\left[\frac{1}{\Delta\omega_0 + \omega - \mathbf{ku} + i(\gamma + \tilde{\gamma}_-)} + \frac{1}{\Delta\omega_0 - (\omega - \mathbf{ku}) + i(\gamma + \tilde{\gamma}_+)}\right] = 0. \tag{2.20}$$

Here

$$v_s = r_{D_e}\omega_{L_i}, \quad \gamma \ll \omega,$$

$$\Delta\omega_0 = \frac{1}{2\omega_0}\left\{\omega_0^2 - \omega_{L_e}^2 - \omega_{L_i}^2 - 3k^2 v_{T_e}^2\right\} \approx \omega_0 - \omega_p\left(1 + \frac{3}{2}k^2 r_{D_e}^2\right).$$

The growth rate γ defined by Eq. (2.20) is maximal in the case $\tilde{\gamma}_\pm \ll \omega$, under decay conditions [14]:

$$\Delta\omega_0(k_d) = \omega(k_d) - \mathbf{k}_d\mathbf{u}. \tag{2.21}$$

In this case

$$\omega(k_d) = k_d v_s, \tag{2.22}$$

$$\gamma = \frac{(k_d r_E)^2}{16 k_d^2 r_{D_e}} \frac{\omega_0 k_d v_s}{\tilde{\gamma}_+ + \gamma_s} - \frac{\tilde{\gamma}_+ \gamma_s}{\tilde{\gamma}_+ + \gamma_s}. \tag{2.23}$$

The instability threshold is determined from (2.23) at $\gamma = 0$:

$$\frac{E_{thr}^2}{4\pi n_e \varkappa T_e} = 16 \sqrt{\frac{\pi}{8}} \frac{v_s(1 - k_d u / k_d v_s)}{v_{T_e} \omega_0} \left\{ \frac{v_{ei}}{2} + \sqrt{\frac{\pi}{8}} \frac{(k_d u_b)^2}{\omega_0^2} \frac{\omega_{L_e}(\omega_{L_e} + k_d u_b)(1 - \omega_0^2/k_d^2 c^2)}{\omega_{L_b} k_d'^3 r_{D_b}^3 (1 - u_b^2/c^2)} \exp\left(-\frac{(\omega_{L_e} + k_d u_b)^2}{2k_d'^2 v_{T_b}^2 (1 - u_b^2/c^2)} \right) \right\} \tag{2.24}$$

$$\left(k_d' = k_d + u_b \frac{k_d u_b (1 - \sqrt{1 - u_b^2/c^2}) - \omega_{L_e} u_b^2/c^2}{u_b^2 \sqrt{1 - u_b^2/c^2}} \right.$$

is the Lorentz-transformed wave vector k_d).

At not too high temperatures, when

$$\frac{u}{v_s} \sim 1,$$

the threshold is minimal for perturbations propagating along the current-velocity direction:

$$\frac{k_d u}{k_d u} = 1.$$

In this case $k u_b > 0$, the contribution of the beam to $\tilde{\gamma}_+$ is small in the experiment, and the threshold is given by ($E_0 \parallel u \parallel k$):

$$\frac{E_{thr}^2}{4\pi n_e \varkappa T_e} = 8 \sqrt{\frac{\pi}{8}} \frac{v_s}{v_{T_e}} \left(1 - \frac{u}{v_s}\right) \frac{v_{ei}}{\omega_0}, \tag{2.25}$$

from which it is seen that the current lowers the parametric-instability threshold.

On the other hand, if the current velocity is small compared with the ion-sound velocity, $u/v_s \ll 1$, then the beam exerts a noticeable influence on the threshold of the parametric instability, and the minimum of the threshold is reached at $k_d u_b / k_d u_b = -1$, $| k_d u_b | \gg \omega_0$:

$$\frac{E_{thr}^2}{4\pi n_e \varkappa T_e} = 8 \sqrt{\frac{\pi}{8}} \frac{v_s}{v_{T_e}} \frac{v_{ei}}{\omega_0} \left\{ 1 - \sqrt{\frac{\pi}{2}} \frac{\omega_{L_e}(k_d u_b - \omega_{L_e})}{\omega_{L_b} k_d'^3 r_{D_b}^3 (1 - u_b^2/c^2)} \frac{(k_d u_b)^2}{\omega_0^2} \left[1 - \frac{\omega_0^2}{k_d^2 c^2} \right] \exp\left(-\frac{(\omega_{L_e} - k_d u_b)^2}{2k_d'^2 v_{T_b}^2 (1 - u_b^2/c^2)} \right) \right\}. \tag{2.26}$$

Figure 20 shows the results of a numerical calculation, which illustrates the dependence of the threshold (2.26) on the beam velocity u_b. The calculations were made for a density $n_e = 10^{21}$ cm^{-3}, which is critical for laser radiation of frequency $\omega_0 = 1.78 \cdot 10^{15}$ sec^{-1}. At $k_d u_b < \omega_{L_e}$ and $k_d u_b > \omega_{L_e}$, respectively, the beam raises and lowers the values of the pump field intensity.

On the other hand, in the absence of a pump field ($E_0 = 0$) the electron beam can excite Langmuir waves if its density is low enough [38]:

$$n_b > \frac{v_{ei}}{2} \frac{m_e}{\pi \sqrt{2\pi e^2}} \frac{k^3 v_{T_b}^3}{\omega_{L_e} |\omega_{L_e} + k u_b|} \exp\left[\frac{(\omega_{L_e} + k u_b)^2}{2k^2 v_{T_b}^2} \right]. \tag{2.27}$$

In the presence of an alternating electric field, the condition on the beam density becomes less stringent:

$$n_b > \frac{v_{ei}}{2} \left(1 - \frac{E_0^2}{E_{thr}^2} \right) \frac{m_e}{\pi \sqrt{2\pi e^2}} \frac{k^3 v_{T_b}^3}{\omega_{L_e} |\omega_{L_e} + k u_b|} \exp\left[\frac{(\omega_{L_e} + k u_b)^2}{2k^2 v_{T_b}^2} \right], \tag{2.28}$$

i.e., even in weak laser radiation, when there is no parametric instability ($E_0^2/E_{thr}^2 < 1$), the field lowers the threshold of the excitation of the Langmuir waves by the electron beam.

3. Effective Collision Frequency in Combined Action of an Electron Beam and a Laser Beam on a Target Plasma

To illustrate the singularities due to the onset of the turbulent stage, we consider here a simple example that demonstrates the possibility of estimating the effective collision frequency, which characterizes the rate of absorption of the energy of the electromagnetic field by the plasma particles. We use the fact that one of the saturation mechanisms of the parametric instability investigated in Sec. 2, wherein the pump wave breaks up into a Langmuir wave and sound, can be the nonlinear shift of the frequency of the natural oscillations of the plasma [39]:
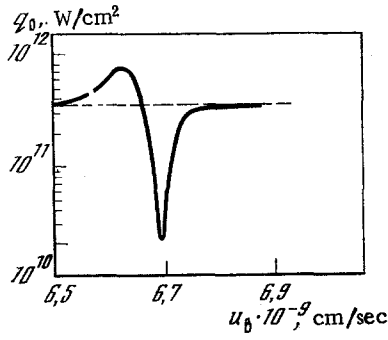
Fig. 20. Threshold of parametric instability (decay of the pump wave into a Langmuir wave and sound) vs the beam velocity u_b. The dashed line shows the threshold in the absence of a beam (u_b = 0, n_b = 0). q_0 = $E_{thr}^2/4\pi$, [W/cm^2]; n = 10^{21} cm^{-3}; T_e = 500 eV; n_b/n_e = 10^{-6}. The values of q_0 along the vertical axis are 10^5 times larger than those indicated.

$$\omega'_p(\mathbf{k}) = \omega_p\left(1 + \frac{3}{2}k^2 r_{D_e}^2\right) + \delta\omega(\mathbf{k}), \qquad (2.29)$$

where the shift $\delta\omega(\mathbf{k})$ is defined by the relation [40]:

$$\delta\omega(\mathbf{k}) = -\frac{\omega_{L_e}}{4}\int\frac{d\mathbf{k}'}{(2\pi)^3}\frac{W_e(\mathbf{k}')}{n_e \varkappa T_e}\frac{(\mathbf{k}\mathbf{k}')^2}{kk'}. \qquad (2.30)$$

Here $W_e(\mathbf{k})$ is the spectral density of the Langmuir-noise energy and is connected with the spectral density of the ion-sound energy by the relation

$$W_e(\mathbf{k}) = \frac{1}{16}\left(\frac{kr_E}{kr_{D_e}}\right)^2\frac{\omega_0^2}{\tilde{\gamma}^2}W_s(\mathbf{k}). \qquad (2.31)$$

Since the frequency shift $\delta\omega(\mathbf{k})$ is negative [see (2.35)], it is clear from (2.29) that the frequency of the natural oscillations of the plasma decreases ($\omega'_p(\mathbf{k}) < \omega_p(\mathbf{k})$) and consequently, the frequency shift causes an increase of the threshold wave number k_m, defined from the decay condition

$$\omega_0 - \omega'_p\left(1 + \frac{3}{2}k_m^2 r_{D_e}^2\right) = k_m v_s. \qquad (2.32)$$

This can eliminate the instability if the instability threshold increases with increasing k. In the case of a plasma with a beam, when the instability threshold is given by (2.26), this is precisely the situation we are dealing with in view of the strong (exponential) dependence of the beam terms on k. We therefore take here the nonlinear frequency shift to be the mechanism that saturates the parametric instability of the plasma with the beam.

The condition for the elimination of the instability ($\gamma = 0$) leads to the equation

$$\frac{E^2}{4\pi n_e \varkappa T_e} = 16\frac{\gamma_s(k_m)\tilde{\gamma}(k_m)}{\omega_0 k_m v_s}, \qquad (2.33)$$

where the wave number k_m is defined by the condition

$$\omega_0 - \omega_p(1 + {}^3/_2 k_m^2 r_{D_e}^2) - \delta\omega(k_m) - k_m v_s = 0. \qquad (2.34)$$

[here and below $\tilde{\gamma} \equiv \tilde{\gamma}_+$ is defined by relation (2.18).] The frequency shift of the natural oscillations with k = k_m is then

$$\delta\omega(k_m) = -\omega_{L_e}\frac{E_e^2}{32\pi n_e \varkappa T_e}, \qquad (2.35)$$

where $\dfrac{E_e^2}{8\pi} = \displaystyle\int\frac{d\mathbf{k}'}{(2\pi)^3}W_e(k')$ is the total energy density of the Langmuir noise.

Recognizing that $\gamma_s(k_m)/k_m v_s = \gamma_s(k_d)/k_d v_s$, we obtain from (2.33)

$$\tilde{\gamma}(k_m) = p^2 v_{ei}/2, \qquad (2.36)$$

where $p^2 = E_0^2/E_{thr}^2$ is the excess above threshold and satisfies the condition

$$1 - \frac{2\tilde{\gamma}_b(k_d)}{v_{ei}} < p^2 < 1.$$

Here

179

$$\tilde{\gamma}_b = \sqrt{\frac{\pi}{8}} \frac{\omega_{L_e}(k_d u_b - \omega_{L_e})(1 - \omega_0^2/k_d^2 c^2)}{\omega_{L_b} k_d'^3 r_{D_b}^3 (1 - u_b^2/c^2)} \frac{(k_d u_b)^2}{\omega_0^2} \exp\left[-\frac{(\omega_{L_e} - k_d' u_b)^2}{2 k_d'^2 v_{T_b}^2 (1 - u_b^2/c^2)} \right],$$

$$(2.37)$$

$$k_d' = k_d + u_b \frac{k_d u_b \left(1 - \sqrt{1 - u_b^2/c^2}\right) - \omega_0^2 u_b^2/c^2}{u_b^2 \sqrt{1 - u_b^2/c^2}}, \quad u_b \parallel -k_d.$$

Equation (2.36) determines the energy density of the Langmuir oscillations $E_e^2/8\pi$, inasmuch as from (2.34) we get, taking (2.35) into account,

$$k_m = \frac{1}{3 r_{D_e}} \left\{ \left[\frac{\omega_{L_i}^2}{\omega_{L_e}^2} + 6 \frac{\omega_0 - \omega_p}{\omega_p} + \frac{3}{16\pi} \frac{E_e^2}{n_e \varkappa T_e} \right]^{1/2} - \frac{\omega_{L_i}}{\omega_{L_e}} \right\}. \qquad (2.38)$$

Under conditions when the excess above threshold p is not too close to unity, so that

$$\left| \ln \frac{\nu_{ei}}{2\tilde{\gamma}_b(k_d)} (1 - p^2) \right| \ll \frac{\omega_{L_e}(k_d u_b - \omega_{L_e})}{k_d^2 v_{T_b}^2} \approx \frac{\omega_{L_e}}{k_d v_{T_b}}$$

the energy density of the Langmuir noise is low:

$$\frac{3}{16\pi} \frac{E_e^2}{n_e \varkappa T_e} \ll 6 \frac{\omega_0 - \omega_p}{\omega_p} \qquad (2.39)$$

and from (2.36) we obtain, taking (2.38) and (2.39) into account,

$$-\frac{\omega_{L_e}(k_d u_b - \omega_{L_e})}{k_d^2 v_{T_b}^e} \frac{\delta k}{k_d} = \ln \left[\frac{\nu_{ei}}{2\tilde{\gamma}_b(k_d)} (1 - p^2) \right], \qquad (2.40)$$

where

$$\delta k = \frac{E_e^2}{32\pi n_e \varkappa T_e r_{D_e}} \left[\frac{\omega_{L_i}^2}{\omega_{L_e}^2} + 6 \frac{\omega_0 - \omega_p}{\omega_p} \right]^{-1/2}. \qquad (2.41)$$

Substituting in the obtained equation the expression for δk, we get the stationary energy density of the Langmuir noise:

$$\frac{E_e^2}{8\pi n_e \varkappa T_e} = 4 k_d r_{D_e} \left[\frac{\omega_{L_i}^2}{\omega_{L_e}^2} + 6 \frac{\omega_0 - \omega_p}{\omega_p} \right]^{1/2} \frac{k_d'^2 v_{T_b}^2 (1 - u_b^2/c^2)}{\omega_{L_e}(k_d u_b - \omega_{L_e})} \ln \left[\frac{\nu_{ei}}{2\tilde{\gamma}_b(k_d)} (1 - p^2) \right]^{-1}. \qquad (2.42)$$

Taking into account relation (2.31) between the spectral energy densities of the Langmuir and ion-sound noises, we obtain

$$\tilde{\gamma}^2(k_m) \frac{E_e^2}{8\pi} = \frac{1}{16} \left(\frac{k r_E}{k r_{D_e}} \right)^2 \omega_0^2 \frac{E_s^2}{8\pi} = p^2 \frac{\nu_{ei}}{2} \gamma_s(k_d) \frac{\omega_0}{k_d v_s} \frac{E_s^2}{8\pi}. \qquad (2.43)$$

We then have for the stationary energy density of the ion-sound noise

$$\frac{E_s^2}{8\pi n_e \varkappa T_e} = 4 \sqrt{\frac{2}{\pi}} \frac{\nu_{ei}}{\omega_{L_i}} k_d r_{D_e} \left[\frac{\omega_{L_i}^2}{\omega_{L_e}^2} + 6 \frac{\omega_0 - \omega_p}{\omega_p} \right]^{1/2} \frac{k_d'^2 v_{T_b}^2 (1 - u_b^2/c^2)}{\omega_{L_e}(k_d u_b - \omega_{L_e})} p^2 \ln \left[\frac{\nu_{ei}}{2\tilde{\gamma}_b(k_d)} (1 - p^2) \right]^{-1}. \qquad (2.44)$$

Knowing the energy density of the noise, we can obtain the effective collision frequency, defined by the relation

$$\nu_{ef} = 4\pi \frac{\omega_0^2}{\omega_{L_e}^2} \sigma_{ef} \equiv \frac{\pi}{2} \frac{\omega_0^2}{\omega_{L_e}^2} \int \frac{d\mathbf{k}}{(2\pi)^3} \frac{(k r_E)^2 \omega_0^2}{E_0^2} \frac{\omega_{L_i}^2}{k v_s} W_s(\mathbf{k}) \left\{ \frac{\tilde{\gamma}_-}{(\Delta \omega_0 + k v_s)^2 + \tilde{\gamma}_-^2} + \frac{\tilde{\gamma}_+}{(\Delta \omega_0 - k v_s)^2 + \tilde{\gamma}_+^2} \right\}. \qquad (2.45)$$

Taking into account relation (2.31) between the spectral densities of the Langmuir and ion-sound noises, and also the fact that $W_e(k)$ has a maximum near the wave number $k = k_m$, which is defined under decay conditions by (2.34), we obtain from (2.45)

$$\nu_{ef} = \tilde{\gamma}(k_m) \frac{E_e^2}{E_0^2}. \qquad (2.46)$$

Substituting E_e^2 in the obtained relations, we get

$$\nu_{ef} = \sqrt{\frac{2}{\pi}} \frac{v_{T_e}}{v_s} \omega_0 k_d r_{D_e} \left[\frac{\omega_{L_i}^2}{\omega_{L_e}^2} + 6 \frac{\omega_0 - \omega_p}{\omega_p} \right]^{1/2} \frac{k_d'^2 v_{T_b}^2 (1 - u_b^2/c^2)}{\omega_{L_e} (k_d'' u_b - \omega_{L_e})} \ln \left\{ \frac{\nu_{ei}}{2\bar{\gamma}_b (k_d)} (1 - p^2) \right\}. \tag{2.47}$$

It is seen from the obtained expression that the effective collision frequency depends little on the excess above threshold and increases with increasing thermal scatter in the beam: $\nu_{ef} \sim v_{T_b}^2$. At an electron temperature $T_e = 500$ eV and a density $n_e = 10^{21}$ cm^{-3}, the effective collision frequency $\nu_{ef} = 10^{13}$ sec^{-1} exceeds the Coulomb collision frequency $\nu_{ei} = 10^{12}$ sec^{-1} by one order of magnitude if $n_b/n_e = 10^{-6}$, $p^2 = 0.9$, $|k_d u_b - \omega_{L_e}| \approx k_d v_{T_b}$ (the beam velocity needed for this purpose is $u_b \approx 10^{10}$ cm/sec at a thermal scatter $v_{T_b}/u_b \approx 0.05$).

To summarize, under certain conditions a relatively weak current and relatively weak beam, acting as "catalysts" of sorts in a plasma are capable of lowering substantially the threshold of parametric instability, and this can lead to a more effective absorption of the laser energy [see, e.g., Eqs. (2.25) and (2.26)]. This conclusion does not contradict experiments in either the microwave band [41] or in the laser band in the case when a CO_2 laser is used to heat the plasma in a plasma focus [42].

On the other hand, as is seen from (2.28), the combined action of electromagnetic radiation and of an REB on a plasma can greatly increase the efficiency of absorption of high-power REB in a target (cf. [5]) without the intolerable heating of the plasma of this target by the reverse current.

4. Gasdynamics of Cumulative Compression of the Target and Transport Processes

After the REB and PLR are absorbed in the corona, the plasma heating should be accompanied by an expansion of the corona. In the case when the electron thermal conductivity encompasses the entire region in which the REB is absorbed and the corona expands, we can obtain the hydrodynamic equations that describe the time variation of the plasma temperature and of the ion density, in the form

$$T = 1{,}4 \cdot 10^{-2} z^{1/2} A^{-1/4} (q_1 \tau_1)^{1/2} \text{ keV}, \tag{2.48}$$

$$n_i = 3 \cdot 10^{10} q_1^{1/2} t^{-1/2} \bar{z}^{-9/4} A^{3/4}, \tag{2.49}$$

where t is the time; A, atomic weight of the target material; $\bar{z}$, charge; and q_1 and τ_1, respectively, flux density and REB pulse duration. From (2.48) and (2.49) it is easy to estimate, e.g., the temperature and pressure near the region where the REB is absorbed in the plasma at beam parameters of the same type as obtained in our plasma focus: temperture T $\simeq 5$ keV and pressure P $\simeq 10^8$ atm. At a plasma-focus beam energy of the order of 1 MJ (which calls for the use of a capacitor bank or an inductive storage rated 5 MJ) the corresponding values are of the order of 40 keV and 10^{10} atm, respectively.

It should be noted that when account is taken of the possible existence of abrupt density gradients in our plasma during this heating stage, and also when account is taken of the results of Secs. 2 and 3, it can be assumed that ion-sound oscillations will build up in the plasma. It is therefore necessary to examine the results of a possible modification of the calculations presented above for the plasma heating, with allowance for the data of [43-45]. It was obtained there that the thermal conductivity coefficient in such a plasma changes by a factor α: $(m_e/M_i)^{1/2} \leqslant \alpha \leqslant (m_e/M_i)^{1/4}$. It is clear that this circumstance may relax the requirements imposed both on the laser when used for preliminary heating of the target in the thermal-wave regime, and with respect to the beam that produces the principal heating; it may lead also to an increase of the transfer coefficient η in the corona.

In fact, the energy released at $n \sim n_{cr}$ is transformed into a flux of heat-conduction electrons directed both towards the center $(-q_t)$ and towards the corona (q_c). In accord with this physical fact, the maximum of the electron temperature is located near the critical density.

As shown by analytic and numerical investigations [2], at laser-radiation flux densities $q \sim 10^{12}$–10^{14} W/cm^2 the plasma region with density $\rho \approx \rho_{cr}$ is directly adjacent to the hydrodynamic discontinuity, i.e., to the jumplike transition from the corona to the dense and cold layer of the target material. The energy flux fed to the discontinuity, $q_t < q_L$, is transformed into a hydrodynamic energy flux directed towards the corona and into work consumed in acceleration in the direction of the center of the dense and cold layer of matter. The last

quantity is the useful part of the total energy supplied, and after the end of the laser pulse it remains in the form of kinetic energy T_{kin} or in the form of energy of motion of the nonevaporated part of the target towards the center. Calculations performed for a thin spherical shell have yielded a maximum ratio $\eta_1^{max} = T_{kin}/q_T\tau_0 \approx 41\%$ for the case of classical thermal conductivity (τ_0 is the duration of the laser pulse). However, since the heat supplied to the discontinuity is $q_t < q_L$, the maximum hydrodynamic efficiency is $\eta = T_{kin}/q_L < \eta_1^{max}$ and amounts, according to numerical calculations, to $\eta \approx 10\text{-}20\%$.

On the other hand, in the case of anomalously low thermal conductivity in the corona the greater part of the energy absorbed near the critical density will obviously be transformed into the work required to accelerate the dense cold matter towards the center.

The necessary condition for any conceivable scheme of pulsed controlled thermonuclear fusion to be effective is that a high final density of the thermonuclear fuel be reached.

As shown by a numerical experiment [2], it is necessary to have a sufficiently high average density $\rho \sim$ g/cm^3, i.e., to attain a degree of compression $\sim 10^3$. The general relation that determines the magnitude of the compression (ρ_f and ρ_0 are the final and initial densities, respectively) is of the form $\delta = (T_{kin}/E^0_{therm})^{1/\gamma-1}$, where E^0_{therm} is the initial thermal energy of the compressed matter, and γ is the adiabatic exponent. Up to the present, three schemes that lead to high compressions have been theoretically investigated. The simplest version is to compress the matter with the aid of a heavy shell. In this case the absorbed energy is transformed during the first stage into the kinetic energy of an external spherical layer whose mass M is much larger than the mass m of the compressed material contained inside the shell. It is easily seen that in this scheme the compression is given by $\delta \sim (M/m)^{1/\gamma-1}$. This method is of interest only to investigations of the physics of the compression and cannot be used to attain high amplification coefficients, since the condition M>>m must be satisfied, and this limits strongly the mass of the thermonuclear fuel and consequently of the thermonuclear yield.

Another well-known scheme of initiating a thermonuclear reaction is to compress and heat homogeneous spherical targets by a radiation pulse or REB that increases strongly with time. The physical idea of this method is to choose a pressure pulse of such form, that the compression and heating of the medium takes place in the absence of shock waves, i.e., in the ultimate isentropic regime. As a result, it becomes possible in principle to attain ultrahigh compressions δ 10^4. This scheme, however, imposes very stringent requirements on the pulse waveform.

The optimum mentioned above can be reached also by using hollow shell targets, constituting an assembly of spherical layers of substances having different physical properties. The degree of compression of matter in targets of this type is determined principally by the geometric factor R/Δ, where R is the outside radius and Δ is the total thickness of the shell, and depends little on the temporal waveform of the pulse.

A detailed physical and numerical analysis has shown that the thermonuclear system is effective only if the spatial distribution of the target plasma parameters ahead of the flash is such that the thermonuclear burning begins at the center of the target and propagates towards the periphery. This means that at the instant preceding the thermonuclear flash there should exist in the center a core heated to the temperature $T_0 \gtrsim 10$ keV and having a density that ensures a high degree of burnup of the thermonuclear fuel in it. If we denote the radius and density of the core by R_0 and ρ_0, respectively, then the thermonuclear energy released in it is determined by the parameter $y_0 = \rho_0 R_0$. If at $y_0 \approx 1$ g/cm^2 the temperature is $T_0 \gtrsim 1$ keV, then the degree of burnup is ~ 1. We note that at $T_0 \approx 10$ keV the total reserve of thermonuclear energy in the DT mixture is 300 times larger than the thermal energy. However, inasmuch as only several percent of the total energy absorbed in the corona is transferred in principle to the center of the target, burnup of only the central core cannot ensure a high amplification coefficient of the system as a whole. Therefore, the mass of the core should amount to only a small fraction of the total mass of the thermonuclear fuel. On the other hand, the total energy released as a result of the thermonuclear flash at the center should be high enough to cause a thermonuclear detonation that involves the total mass of the fuel. Thus, the initiation problem reduces to separation of the center at an optimal ratio of the central mass and the main mass.

The total efficiency of the system is determined by the ratio of the average density to the total mass of the thermonuclear fuel in the target. The product ρR for the target as a

whole should be close to unity. The reason is that the burning of the system is effective if the α particles are strongly decelerated in the thermonuclear fuel. We note that the total capture of α particles and neutrons takes place at $\rho R = 0.15$ and $\rho R = 8$, respectively.

New possibilities are offered by the use of a plasma focus to realize the schemes indicated above. In fact, first, it must be borne in mind that approximately half the energy of the plasma focus bank goes over into kinetic energy of the collapsing current sheath. Usually only a small part of this energy ($\simeq 10\%$) goes over into thermal energy of the plasma during the instant of the first compression. It is easy to calculate, however, that in the case when a cylindrical target placed at the center along the chamber axis is used, the energy flux to the surface of this cylindrical target, with diameter $\lesssim 1$ mm, amounts in our case to 10^{12} W/cm^2, and if the storage bank has an energy $\sim 1-5$ MJ, values of the order 10^{14} W/cm^2 can be obtained within a time of action of the order of several nanoseconds. This means that one can count on pressures of the order of 10^7-10^8 atm; by suitable choice of the composition and shape of the targets, this will make possible target compression to densities of the order of 10 g/cm^3. This figure can be increased by a special choice of the shape of the density profile, as shown by numerical calculation [46].

Next, inasmuch as the magnetic fields in the plasma focus are of the order of 1 MG, and at a bank rating 5 MJ this value can increase to about 10 MG, the requirement stated above concerning the total capture of the α particles is decreased by at least one order of magnitude. This condition means that in such a scheme one can work with cylindrical targets of relatively small diameter.

It is also clear that the magnetization of the electronic thermal conductivity improves the burning conditions for this cylindrical target. In contrast to the burning conditions of spherical laser targets, where the reactions are initiated only at the center, in our case burning due to capture of α particles and neutrons can be maintained by a relativistic electron beam.

We note that by virtue of the rather high symmetry that experiment yields for the compression of the plasma in the plasma focus, the instability of the compression of cylindrical targets is determined only by the precision with which they are produced.

Thus, the combined action of PLR and REB on thermonuclear targets uncovers many new possibilities of both plasma heating and the design of the targets themselves. The system energy requirements are less stringent than in the classical schemes of pulsed controlled thermonuclear fusion based on PLR or on REB. In particular, with plasma-focus bank energy $4 \cdot 10^4$ J and using solid targets of special constructions, one can hope to obtain a neutron yield up to 10^{12} neutrons/pulse. Increasing the plasma-focus bank (and consequently also the REB) leads to an increase in the neutron yield approximately in accord with the similarity law that holds in laser thermonuclear fusion [1]. The latter, however, can be attained by simpler means compared with pure laser methods.

It is clear, however, that to determine all these possibilities it is necessary to investigate experimentally the combined interaction of PLR and REB with a plasma and on acceleration of shells in a plasma focus, as well as theoretical investigations aimed at determining the optimal systems of corona heating and burning of cylindrical targets with complicated composition.

In conclusion, the authors thank V. P. Novikov for help with startup of the laser, and V. T. Tikhonchuk and Yu. V. Bychenkov for a discussion of the results of Secs. 1-3.

LITERATURE CITED

1. N. G. Basov and O. N. Krokhin, Zh. Eksp. Teor. Fiz., 45, No. 1, 171 (1964).
2. Yu. V. Afanas'ev, N. G. Basov, P. P. Volosevich, et al., Plasma Physics and Controlled Nuclear Fusion Res., IAEA, CN-33/PD-3, Tokyo, Japan (1974).
3. I. Nuckolls, L. Wood, A. Thiessen, and G. Zimmerman, Nature, 239, No. 5368, 139-142 (1972).
4. F. Winterberg, Nucl. Fusion, 12, No. 3, 353-363 (1972).
5. N. V. Babykin, E. K. Zavoiskii, A. A. Ivanov, and L. I. Rudakov, Plasma Physics and Controlled Nuclear Fusion Res., IAEA, CN-28/D-10, Madison, USA (1971).
6. L. I. Rudakov, Yu. V. Koba, V. I. Liksonov, et al., Plasma Physics and Controlled Nuclear Fusion Res., IAEA, CN-33/F2-1, Tokyo (1974).
7. J. Chang, M. J. Clauser, J. R. Freeman, et al., Plasma Physics and Controlled Nuclear Fusion Res., IAEA, CN-33/F2-2, Tokyo, Japan (1974).

8. N. G. Basov, O. N. Krokhin, G. V. Sklizkov, et al., Zh. Eksp. Teor. Fiz., 62, No. 1, 203 (1972).
9. N. G. Basov, E. G. Gamalii, O. N. Krokhin, et al., Laser Interaction and Related Plasma Phenomena, Vol. 3B, Plenum Press (1977), New York, p. 553.
10. N. G. Basov, O. N. Krokhin, G. V. Sklizkov, and S. I. Fedotov, Preprint Fiz. Inst. Akad. Nauk SSSR, No. 51 (1974).
11. V. A. Gribkov, O. N. Krokhin, G. V. Sklizkov, N. V. Filippov, and T. I. Filippova, Pis'ma Zh. Eksp. Teor. Fiz., 18, No. 9, 541 (1973).
12. V. A. Gribkov, O. N. Krokhin, G. V. Sklizkov, N. V. Filippov, and T. I. Filippova, Pis'ma Zh. Eksp. Teor. Fiz., 18, No. 1, 11 (1973).
13. V. I. Agafonov, I. F. Belyaeva, V. V. Vikhrev, et al., Plasma Physics and Controlled Nuclear Fusion Res., IAEA, CN-28/D-6, Madison, U.S.A. (1971).
14. V. P. Silin, Parametric Action of High-Power Radiation on a Plasma [in Russian], Nauka, Moscow (1973)
15. N. G. Basov, V. A. Gribkov, O. N. Krokhin, and G. V. Sklizkov, Zh. Eksp. Teor. Fiz., 54, No. 4, 1073 (1968).
16. V. A. Gribkov, O. N. Krokhin, and G. V. Sklizkov, Preprint Fiz. Inst. Akad. Nauk SSSR, No. 136 (1973).
17. Yu. V. Afanas'ev and O. N. Krokhin, in: Physics of High Energy Densities [Russian translation], Mir, Moscow (1974).
18. N. G. Basov, V. A. Gribkov, A. I. Isakov, et al., Preprint Fiz. Inst. Akad. Nauk SSSR, No. 16 (1975).
19. N. G. Basov, O. N. Krokhin, A. A. Rupasov, et al., Preprint Fiz. Inst. Akad. Nauk SSSR, No. 47 (1973).
20. V. A. Gribkov, G. V. Sklizkov, S. I. Fedotov, and A. S. Shikanov, Prib. Tekh. Eksp., No. 4, 213 (1970).
21. N. G. Basov, O. N. Krokhin, N. G. Kryukov, et al., Kvantovaya Elektron., 1, No. 6, 1428 (1974).
22. N. G. Basov, A. E. Danilov, O. N. Krokhin, et al., Preprint Fiz. Inst. Akad. Nauk SSSR, No. 30 (1976).
23. M. J. Lubin and I. M. Soures, J. Appl. Phys., 44, No. 1, 347-350 (1973).
24. N. N. Zorev and S. I. Fedotov, Preprint Fiz. Inst. Akad. Nauk SSSR, No. 123 (1973).
25. A. Saleres, D. Cognard, and F. Floux, Fifth Eur. Conf. Controlled Fusion and Plasma Phys., Vol. 1, Grenoble, France (1972), p. 59.
26. H. Van Rohmann, Z. Phys., 15, 510-512 (1914).
27. L. S. Birks, Rev. Sci. Instrum., 41, No. 8, 1129-1132 (1970).
28. A. V. Vinogradov, I. I. Sobel'man, and E. A. Yukov, Kvantovaya Elektron., 2, 6, 1165-1170 (1975).
29. L. P. Presnyakov, Usp. Fiz. Nauk, 119, No. 1, 49 (1976).
30. E. V. Aglitskii, V. A. Boiko, A. V. Vinogradov, and E. A. Yukov, Preprint Fiz. Inst. Akad. Nauk SSSR, No. 45 (1973).
31. V. A. Gribkov, Int. Conf. Energy Storage, Compression and Switching, Torino, Italy (1974).
32. B. N. Brejzman and D. D. Ryutov, Nucl. Fusion, 14, No. 6, 873 (1974).
33. N. G. Basov, Paper at Eighth Internat. Conf. on Laser Thermonuclear Fusion, Rynia (near Warsaw), Poland (19-24 May 1975).
34. N. G. Basov, Yu. S. Ivanov, O. N. Krokhin, et al., Pis'ma Zh. Eksp. Teor. Fiz., 15, 10 (1972).
35. G. Yonas, J. W. Poukey, K. R. Prestwich, et al., Nucl. Fusion, 14, 731 (1974).
36. P. S. Erokhin and S. V. Moiseev, Zh. Eksp. Teor. Fiz. 65, 143 (1973).
37. Yu. V. Afanas'ev, V. A. Gribkov, and O. N. Krokhin, Abstracts, Third All-Union Conf. on Physics of Interaction of Optical Radiation with Condensed Media, Leningrad (1974).
38. V. L. Ginzburg and A. A. Rukhadze, Waves in a Magnetoactive Plasma [in Russian], Nauka, Moscow (1970).
39. V. Yu. Bychenkov, V. V. Pustovalov, V. P. Silin, and V. T. Tikhonchuk, Preprint Fiz. Inst. Akad. Nauk SSSR, No. 164 (1972).
40. L. M. Gorbunov and A. M. Timembulatov, Zh. Eksp. Teor. Fiz., 53, 1492 (1967).
41. G. R. Johnston, Phys. Fluids, 17, 416-418 (1974).
42. S. Kaliski et al., Paper at Ninth Int. Conf. on Laser Plasma, Warsaw, Poland (1975).
43. S. I. Braginskii, in: Problems in Plasma Theory [in Russian], No. 1, M. A. Leontovich (editor), Atomizdat, Moscow (1973).

44. A. A. Ivanov, Physics of Nonequilibrium Plasma [in Russian], Atomizdat, Moscow (1977).
45. V. A. Gribkov, O. N. Krokhin, V. Ya. Nikulin, et al., Kvantovaya Elektron., $\underline{2}$, No. 5, 975-988 (1975).
46. B. Freeman, J. Luce, and H. Sahlin, Proc. Fifth Eur. Conf. Controlled Fusion and Plasma Physics, No. 68 (1972), p. 68.